Variability in the Characteristics of InGaAsSb/InAs Tunnel FETs Caused by Dopant-induced Traps

S. Sant[1], Q. Ding[1,2], M. Rau[1], M. Luisier[1], and A. Schenk[1]

[1]Integrated Systems Laboratory, ETH Zurich, 8092, Zurich, Switzerland. [2]RWTH Aachen, Aachen, Germany

Abstract

In this paper, an attempt is made to understand the dopant-induced traps near the hetero-interface as a source of variability in InGaAsSb/InAs Tunnel FETs (TFETs). Comparing simulated and measured variability data suggests that a characteristic energy η = 50 meV of the induced density-of-states (DOS) tail yields the best match with the experimental distribution of the sub-threshold swing (SS). Density Functional Theory (DFT) calculations of alloy supercells containing a randomly placed dopant confirm that alloy randomness indeed gives rise to band tails with a significantly larger η compared to that in pure semiconductors.

(Keywords: Tunnel FET, variability, trap-assisted tunneling, alloy band tails)

Introduction

Recent reports [1] have demonstrated that a high on-current together with a sub-60mV/dec SS is achievable in All-III-V TFETs. TCAD analysis of an InGaAsSb/InAs TFET has revealed the degradation of the swing due to trap-assisted tunneling (TAT) caused by single traps at the hetero-interface [2]. Another analysis attributed the poor SS to band tails in the source region [3]. Physical characterization of numerous of such TFETs [4] shows a large variation in swing, threshold voltage, on-current, as well as I_{60} (maximum source current at which the swing is below 60 mV/dec). Such a variability is detrimental to TFET application in low-power logic circuits. The present study aims at understanding the origin of the observed variability in these state-of-the-art TFETs.

In bulk, statistical averaging of the defect states gives rise to a quasi-continuum of tail states – also called band tails. Such an averaging approach loses validity at the nano-scale when there are just a few defects in the active region. Thus, continuous band tails can hardly explain the observed variability. Instead, the latter could originate from the random location of single traps near the hetero-interface, as shown in Fig. 4 of Ref. [2]. However, this does not explain the observed variations of on-current, V_{TH}, or I_{60}. We believe that the actual picture is somewhere in-between a single-trap model and a continuum model of band tails.

In this work, we propose that

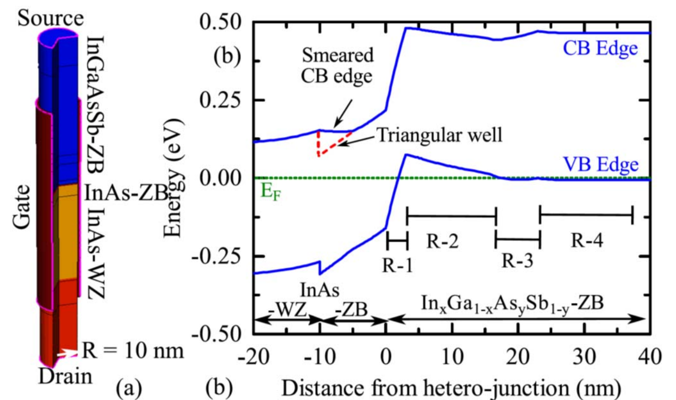

Figure 1: (a) Diagram of an InGaAsSb/InAs nanowire TFET studied in this paper. (b) Band diagram along the axis of the nanowire. Taken from [2].

dopant-induced energy levels in the band gap take part in TAT. It is assumed that these energy levels follow an exponential random distribution as observed in PL measurements [7].

Drift-diffusion simulation study

We performed 3D drift-diffusion simulations of the InGaAsSb/InAs TFET (Fig. 1(a)) using the commercial TCAD package S-Device [5]. The TFET consists of n-doped (N_D = 1x10^{19} cm^{-3}) WZ-InAs drain, intrinsically doped (N_D = 1x10^{17} cm^{-3}) WZ-InAs/ZB-InAs channel, and a p-doped (N_A = 1x10^{19} cm^{-3}) ZB-$In_xGa_{1-x}As_ySb_{1-y}$ source with a composition grading towards the hetero-interface. Such a composition grading was applied in the simulations, which results in the band diagram shown in Fig. 1(b). The same simulation set-up as the one employed in our earlier work [2] was used here. At a p-doping of 1x10^{19} cm^{-3}, there are approximately nine dopant atoms present in the 3 nm thick InGaAsSb disc adjacent to InAs-ZB. We place nine acceptor-like “single traps” in the same disc to match the dopant concentration. To mimic the random location of the dopants, the trap

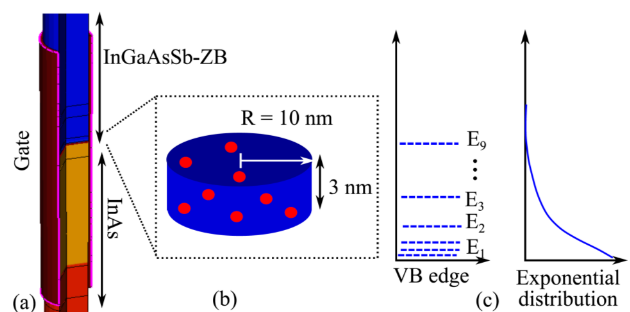

Figure 2: (a-b) Randomly placed dopants are introduced near the hetero-interface. (c) Trap energy levels are taken from an exponential random distribution.

positions are obtained from a uniform random distribution in the disc (see Fig. 2(a)). The energy level of each of the nine traps is a random number chosen from an exponential distribution with a characteristic energy η starting from the valence band edge (see Fig. 2(b)). These traps, when occupied, add a negative point charge at their location which enters the Poisson equation. In this way, the formation of "band tails" from the dopant-induced defect states is modeled at the nano-meter scale. To find a statistical distribution of the device characteristics, fifty such devices were simulated in 3D with the trap locations and energy levels generated by the procedure described above.

Note, that only the dopant-induced traps in the region R-1 near the hetero-interface are considered in the TCAD simulations. This region has the steepest band edges, and traps in this region contribute most to TAT. Dopant-induced traps in the rest of the device are dormant in TAT, but their electrostatic effect is accounted in the simulations by introducing uniform background dopant charges as typically done in TCAD.

Simulation results and discussion

SS, I_{60}, and I_{ON} were obtained from the transfer characteristics of the fifty simulated devices. Different simulation runs were performed for η = 9, 30, and 50 meV. Histograms of the three extracted quantities (based on 50 devices) were plotted for each run. These histograms were then compared with the histograms of the values of *SS*, I_{60} and I_{ON} extracted from the experimental transfer characteristics of different devices. A comparison of these histograms is shown in Figs. 3, 4, and 5. The

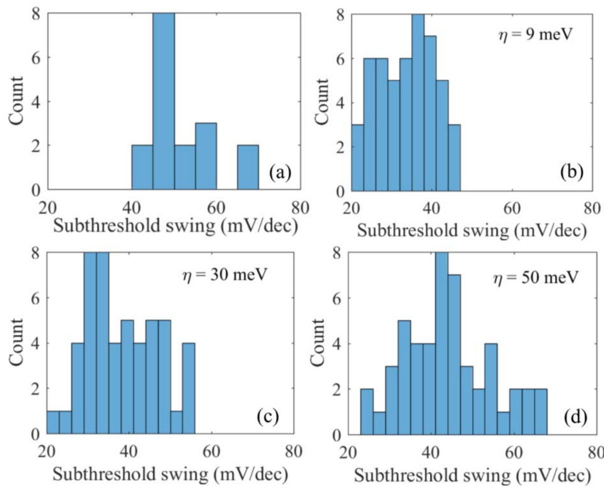

Figure 3: Histogram showing variability of the SS in (a) experimental I_D-V_{GS} data and (b-d) simulated devices with the tail energy η = 9 meV, 30 meV, 50 meV.

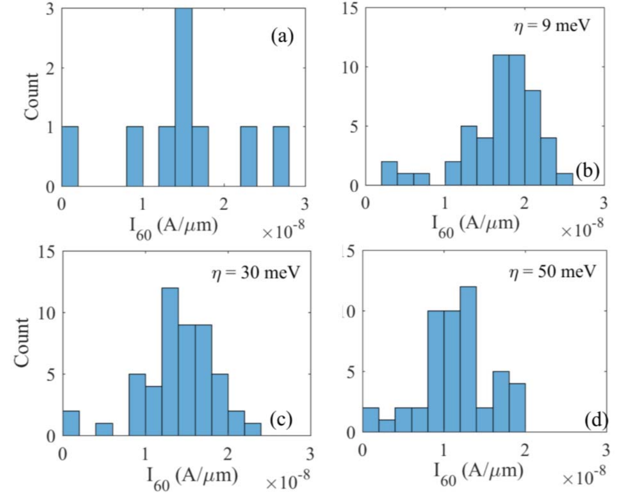

Figure 2: Histogram showing variability of I_{60} in (a) experimental I_D-V_{GS} data and (b-d) simulated devices with the tail energy η = 9 meV, 30 meV, and 50 meV.

simulations suggest that the variability of the swing increases with increasing η. Randomness of the spatial location and energetic position moves the trap state into or out of the tunnel window which gives rise to TAT with different intensities. However, the variability of I_{60} and of I_{ON} depends weakly on η. Both the quantities are dominated by band-to-band tunneling and not TAT. Therefore, they are mainly affected by variations in the electrostatics (arising from random trap placement), but not by TAT. The change in the electrostatics due to the presence of charged traps is small due to the screening by mobile charges. The variability of *SS* cannot be explained with η = 9 meV, only $\eta \approx$ 50 meV fairly reproduces the experimental data. Such a large value of η has not been observed in bulk InAs. A possible origin for band tails with $\eta \approx$ 50 meV is provided below.

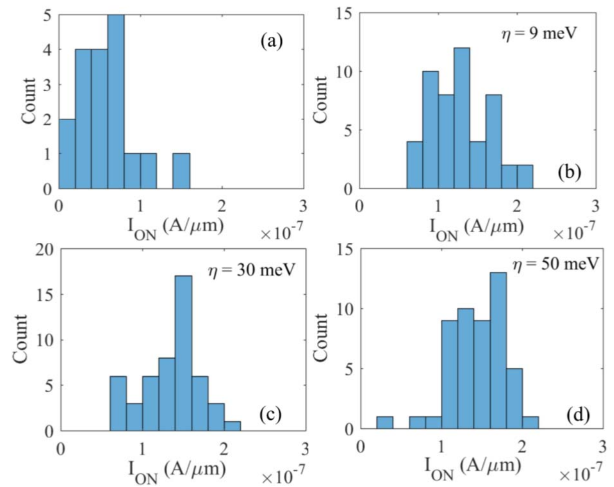

Figure 5: Histogram showing variability of I_{ON} at V_{GS} = 300 mV in (a) experimental I_D-V_{GS} data and (b-d) simulated devices with the tail energy η = 9, 30, 50 meV.

DFT calculations

In order to confirm the hypothesis that the considered dopant-induced traps exist in an InGaAsSb alloy and yield an exponential tail, we performed first-principle electronic structure calculations using the DFT package CP2K [6]. A cubic InAs supercell with 216 atoms was used in the simulations. The actual composition of $In_{0.7}Ga_{0.3}As_{0.84}Sb_{0.16}$ was obtained by randomly replacing 33 In atoms with Ga and 17 As atoms with Sb. The lattice constant for the supercell was determined by varying its side length until the one was found that minimizes the energy. Four such random configurations were used. In each of them, one of the In or Ga atom was replaced by a Zn dopant atom. Four cases of such a "doped" supercell were created from each of the above configurations. Geometric optimization was performed on the dopant atom and its 16 neighbouring atoms, keeping the rest of the atoms constrained in all 16 configurations. This accounts for the distortion of the lattice in the surroundings of the dopant atom.

Electronic structure calculations were performed to extract the energy levels close to the VB edge. The trap levels were identified from the DFT wave functions. As shown in Fig. 7, a VB state is delocalized over the entire supercell while a trap wave function is localized near a Zn atom. A histogram of the trap energy levels of the 16 simulated configurations is shown in Fig. 6. It shows an exponential decay of the trap level density in the band gap with a characteristic energy of η = 24 meV. This value of η is much larger than the η = 9 meV found for bulk InAs [7,8] despite the fact that the alloy is close to InAs in composition. The value is large because the neighborhood of a Zn atom is different in each supercell due to the random

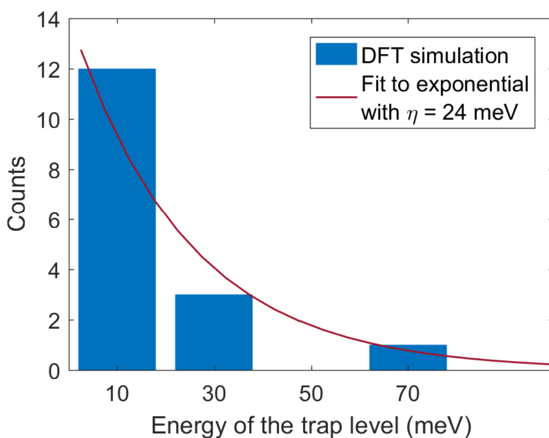

Figure 6: Histogram of the distribution of trap energy levels extracted from the DFT calculations.

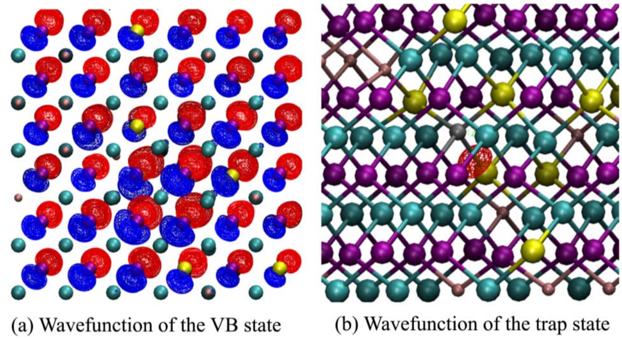

Figure 7: Wave functions of (a) a VB edge state and (b) a trap state in a representative supercell. The trap wave function is strongly localized near a zinc atom.

positions of In, Ga, As, and Sb atoms. As a result, the trap energy level in each of the configurations is different. Thus, the alloy randomness gives rise to stronger band tails. Although the η–value obtained by DFT is quantitatively different from the TCAD estimate, it confirms that alloy randomness can result in an η significantly larger than 9 meV observed in the pure semiconductor.

Conclusion

We tried to understand whether dopant-induced traps near the hetero-interface can be a source of variability in InGaAsSb/InAs TFETs. Their locations were randomized and their energy levels were obtained from an exponential distribution with characteristic energy η. Fifty such devices were simulated for each η. The histograms obtained from the simulations suggest that η = 50 meV results in the best match with the experimental distribution of the swing. DFT calculations of the alloy supercell with a dopant atom confirm that alloy randomness indeed gives rise to band tails with a significantly larger η compared to that in pure semiconductors.

Acknowledgments

The authors gratefully acknowledge Dr. E. Memisevic and Prof. L.-E. Wernersson for providing the statistical data of the TFETs.

References

[1] Memisevic et al, Nano Lett. vol. 17, p. 4373 (2017).
[2] Sant et al, ISTE Nanoelec. Dev., vol. 1, p. 1 (2018).
[3] Memisevic et al, IEEE EDL, vol. 38, p. 1661 (2017).
[4] Memisevic et al, IEEE TED, vol. 64, p. 4746 (2017).
[5] Sentaurus-Device User Guide, Version 2015.06, (2015).
[6] CP2K version 5.0, the CP2K developers' group (2016).
[7] J. R. Dixon and J. M. Ellis, Phys. Rev. 123, 1560 (1961).
[8] Malyutenko et al, Semicond. Sci. Techol. 9, 1047 (1994).